ELSEVIER

Earth and Planetary Science Letters 133 (1995) 517–532

EPSL

Tomographic imaging of lithospheric structures under Taiwan

Ruey-Juin Rau, Francis T. Wu

Department of Geological Sciences State University of New York at Binghamton, Binghamton, NY 13902, USA

Received 15 September 1994; accepted 23 March 1995

Abstract

Tomographic images of the crustal and mantle velocity structures under Taiwan are obtained by simultaneous inversion of local earthquake P-wave arrival times for hypocenters and P-wave velocity structures. In northern Taiwan, a high-velocity zone, coinciding with the Wadati-Benioff zone, can readily be identified as the subducted Philippine Sea plate. The imaged zone dips toward the north at an angle of 40° from a depth range of 20–55 to 100–130 km. An upper-mantle low-velocity wedge, ranging from 40 to 80 km in depth, exists above the subducted slab. Above this wedge is the Ilan Plain of northern Taiwan which lies at the west end of the Okinawa Trough, a well recognized back-arc basin; the crustal velocities under the Plain are also relatively low. The well-defined high-velocity zone and the low-velocity wedge provide some constraints on the thermal structures of the subduction system under northern Taiwan. In tomographic images across the central section of Taiwan, thickening of the crust and up-arching of the lower-crustal materials under the Central Range are commonly observed; the crust under the Western Foothills region is clearly thinner and the near-surface low-velocity layers are well developed. The structures under the Central Range show that although the Taiwan orogeny is quite young, a root, deeper in the north and shallowing to the south, has formed. The results of our tomography show that a significant portion of the lithosphere is involved in the Taiwan orogeny.

1. Introduction

The Taiwan mountain range was created by the collision between the Eurasian Plate and the Philippine Sea Plate (Fig. 1); the collision began at about 4 mybp [1]. The overall plate configuration in the vicinity of Taiwan, as defined by seismicity, is well understood [1,2]. The NW-dipping Ryukyu subduction zone becomes E–W-trending and N-dipping as it dives partially under northern Taiwan. The E-dipping North Luzon seismic zone extends northward to southern Taiwan. The central part of Taiwan, however, is underlain by only shallow seismicity (< 50 km) and a collision is taking place in this section. Near Taiwan, the relative plate motion between the Eurasian Plate and the Philippine Sea Plate is in the direction of N50°W and at an estimated rate of 7.1 cm/yr [3]. This motion is responsible for the collision tectonics of Taiwan.

The seismicity, the rate of uplift [4], and the geodetically measured deformation [5] all indicate that the ongoing tectonics in and around Taiwan is very active. Heretofore, relatively little was known about the crustal and upper-mantle structures, and, as a result, it is frequently assumed that the orogeny is a very superficial process, involving only the Cenozoic sediments in the upper part of the crust [6]. Previously, one-dimensional structures along several profiles were determined [2]; it was found that the crust under the eastern Coastal Range is relatively thin (20 km) and the velocities are close to those of a typical oceanic crust. In contrast, the crusts under the West-

SSDI 0012-821X(95)00076-3

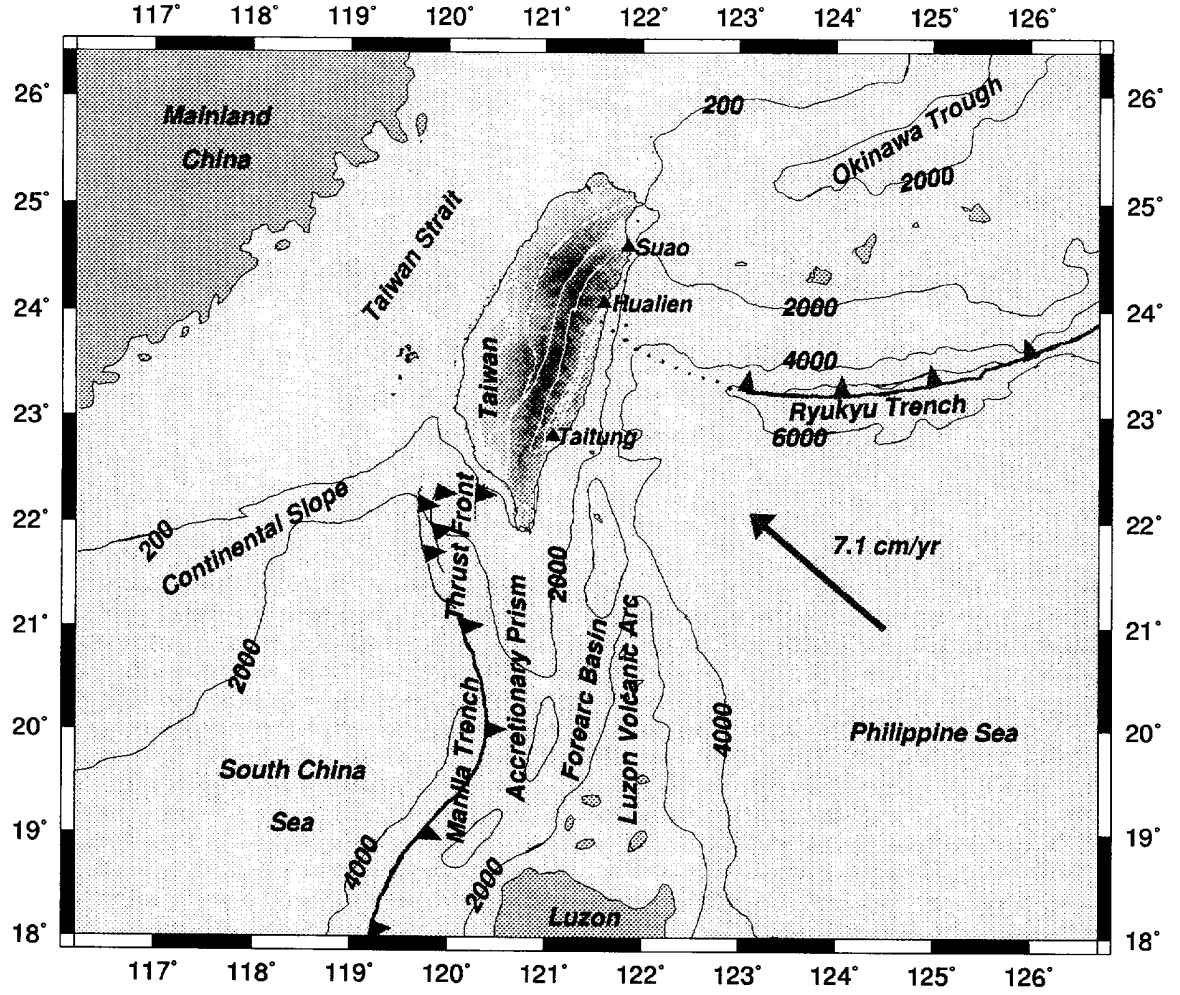

Fig. 1. Topography, bathymetry and tectonic setting of Taiwan and surrounding area (modified from [6]). The locations of the Ryukyu Trench to the east and the Manila Trench to the south are indicated. The vector of relative motion between the Philippine Sea plate and the Eurasian plate is shown by the arrow [3]. The dark area on the island is mountainous, with its highest peak at 3997 m. A small, triangular depression in northeastern Taiwan is the Ilan Plain. It lies at the west end of the Okinawa Trough. The Ryukyu Trench is assumed to continue westward along the dotted line [25]; in some previous work (e.g., [24]) the trench has been assumed to bend sharply northward near Taiwan and connect to Suao. The main geological divisions of Taiwan are demarcated by white lines. The isobaths (in m) outline the morphology of the Chinese continental shelf, slope and the other features.

Fig. 2. Map (top) and 3-D (bottom) views of three grid configurations used in our 3-D inversions. (a) EW–NS oriented grid system for the northern third of Taiwan. (b) Grid system with the horizontal orthogonal directions parallel (N20°E–S20°W) and perpendicular (S70°E–N70°W) to the strike of the island in the northern two-thirds of Taiwan. (c) EW–NS grid system for the whole island. ▲ = CWBSN and TTSN seismic stations; ○,● = original earthquake locations used in each system for map and 3-D views, respectively; ● = nodes (points where the lines cross) in the map view, at the intersections of the grid lines in the 3-D view. *A–A′* through *F–F′* indicate the positions of the tomographic profiles shown in Fig. 4. The selected sections are shaded vertically in the 3-D views. The geological provinces of Taiwan are: *I* = Coastal Plain (CP); *II* = Western Foothills (WF); *III* = western Central Range (WCER); *IV* = eastern Central Range (ECER); *V* = Longitudinal Valley (LV); *VI* = Coastal Range (COR).

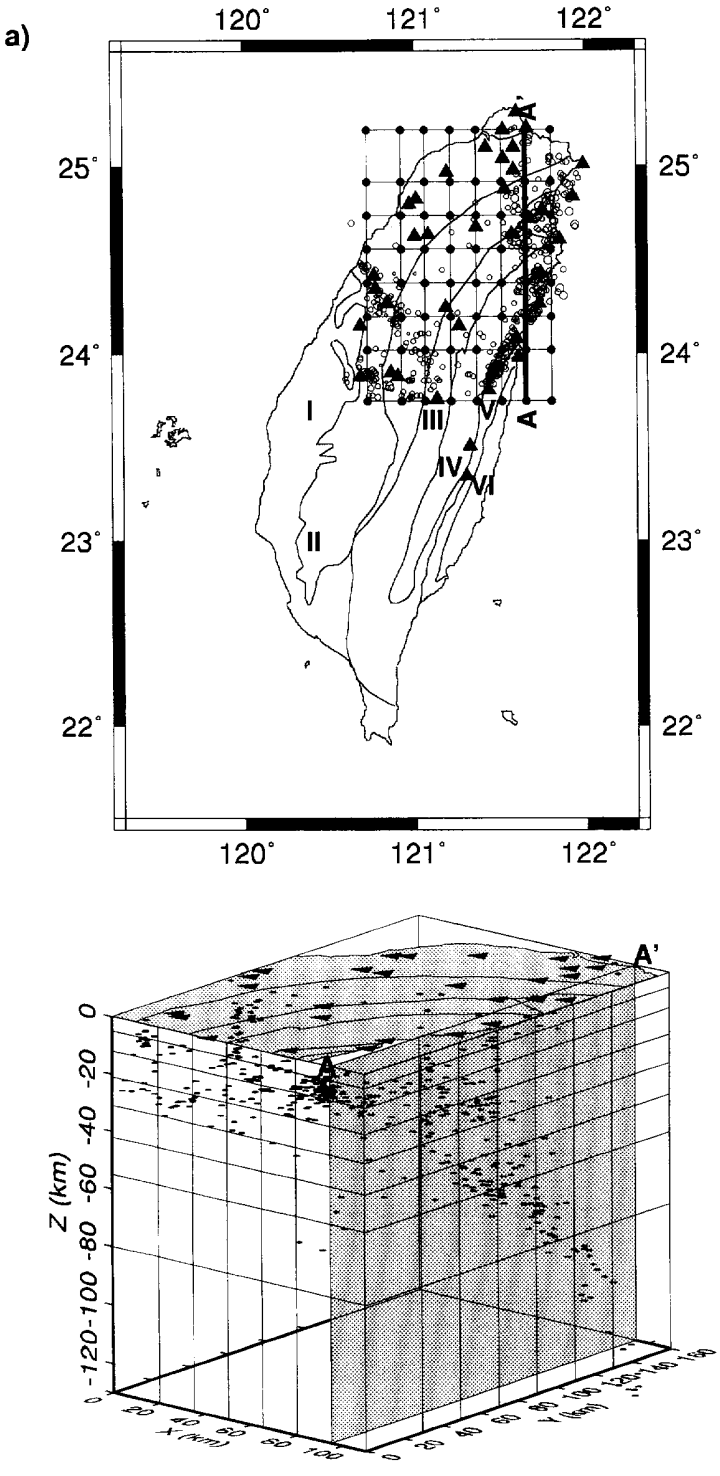
a)
120°
121°
122°
25°
24°
23°
22°
A
A'
I
II
III
IV
V
VI
A'
A
Z (km)
0
-20
-40
-60
-80
-100
-120
0
20
40
60
80
100
X (km)
0
20
40
60
80
100
120
140
160
Y (km)

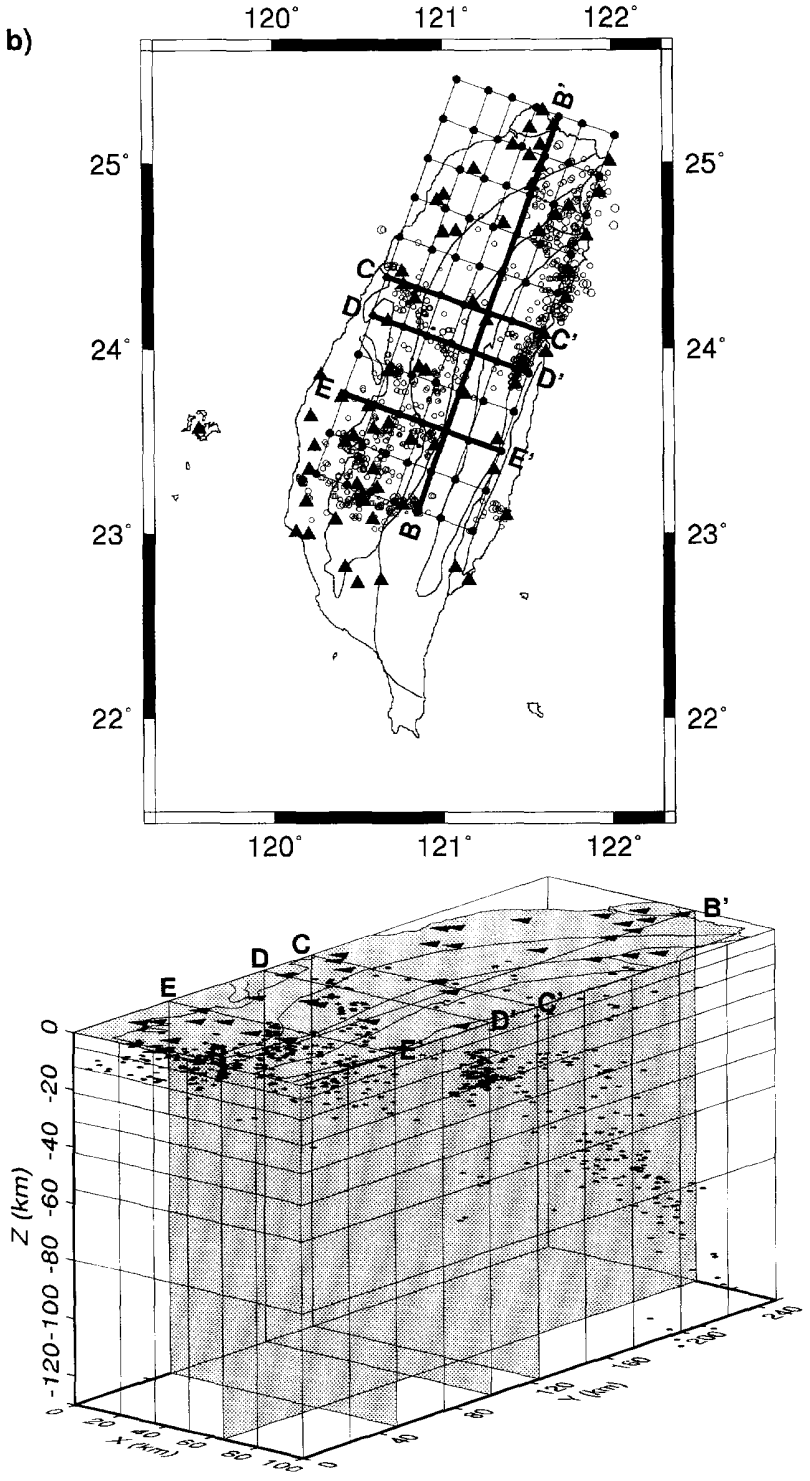

Fig. 2 (continued).

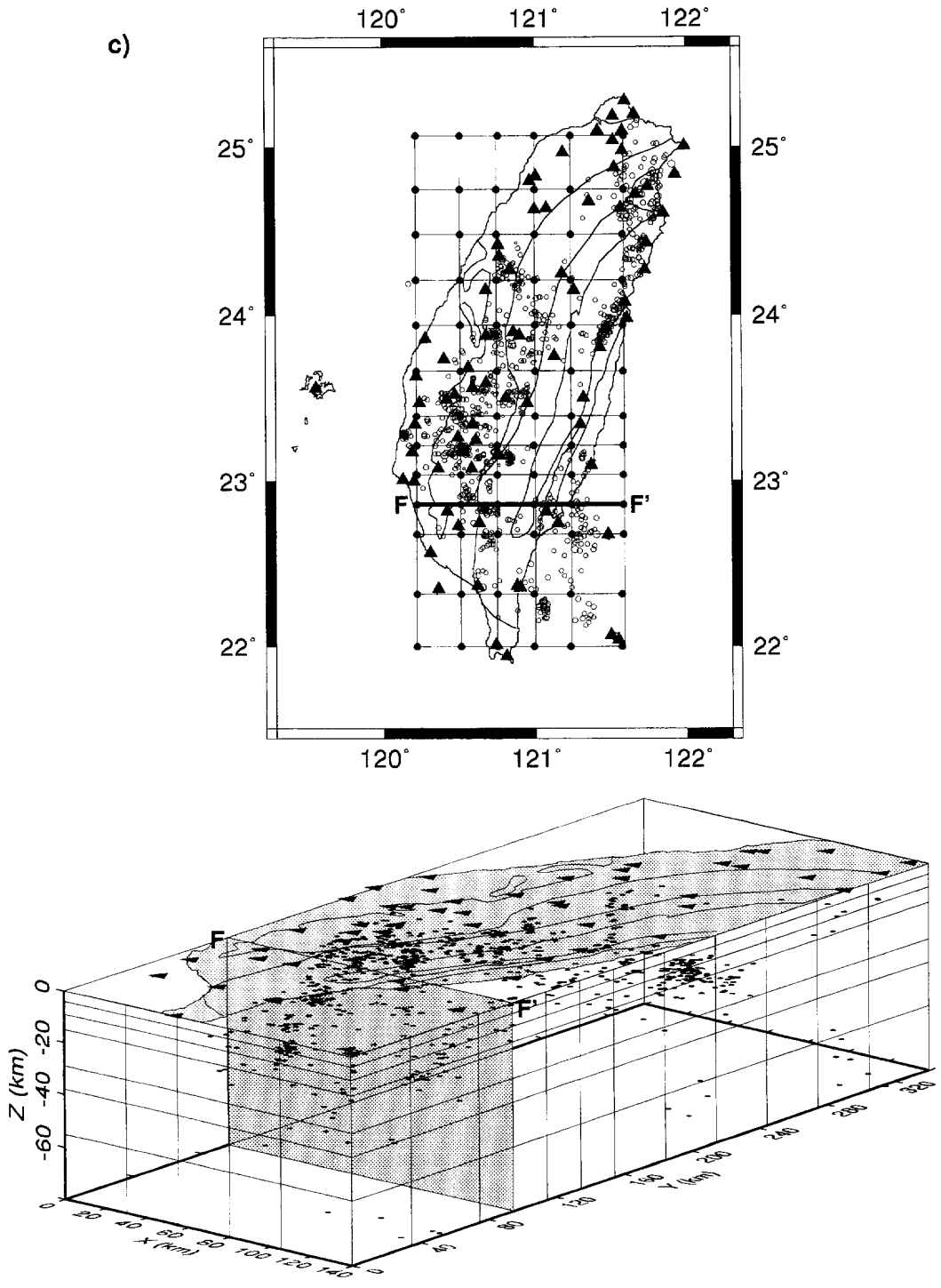

Fig. 2 (continued).

ern Foothills and the Central Range are both continental in nature, but the Moho under the Foothills is about 25 km and that under the Central Range is deepened to about 34 km. Three-dimensional velocity structures under Taiwan were determined by Roecker et al. [7] and Yeh et al. [8]. The resolution of these studies was limited by the sparse network and the precision of arrival time data. Nevertheless, Yeh et al. were able to define a shallow (< 6 km) low-velocity zone under the Ilan Plain area of northern Taiwan, and Roecker et al. mapped large-scale velocity anomalies under the whole island. But much of this relatively small and highly complex collision zone has not yet been mapped in any detail. We now attempt to study the subsurface structures under Taiwan in greater detail. Through this work, we wish to address the following two tectonics-related problems.

First, although the existence of the subduction system under northern Taiwan has been known for some time, some aspects of it remain unclear. For example, in the absence of detailed offshore multichannel seismic data, it is not yet possible to place the intersection of the "trench" with the island based on diffuse seismicity; this is necessary in order to know the precise geometry of the interacting plates near Taiwan. With tomography we can map the subsurface configuration of the subduction zone and extrapolate it for a short distance to the surface to find the "trench". Also, the Okinawa Trough, a back-arc basin, extends morphologically southwestward into northern Taiwan; the Trough narrows westward to form the triangular Ilan Plain, with its opening to the east. Judging from focal mechanisms (e.g., [1]), N–S extension is taking place under and offshore of the Plain. It appears that a back-arc basin is being formed in northern Taiwan. If so, tomographic images of northern Taiwan will allow us a rare opportunity to study the structures under a nascent back-arc basin in some detail.

The second problem is the search for deep structures under the Central Range associated with the collision tectonics. As the collision is younging toward the south [9], changes in subsurface structures from northern to southern Taiwan may show the manner in which the crust responds to tectonic deformation as a function of time. The crustal structures provide undoubtedly the best records of the large-scale strain sustained in the mountain building processes. In the thin-skinned tectonics modeling of the Taiwan orogeny [6], little thickening of the crust is expected, and the orogeny involves only Tertiary sediments from the Coastal Plain to the Central Range. But the existence of the sedimentary wedge extending across the Central Range has never been demonstrated and the passive role of the crust and upper mantle in the process is also assumed. Although we know from earlier work [2] the general changes in crustal structures across the island, details are lacking. Through tomography we wish to determine whether there is a deepening sedimentary wedge under the Central Range [6], and whether any significant structures exist in the crust and the upper mantle that might be related to the orogeny.

Detailed tomography is made possible by the recent expansion, in 1991, of the telemetered network on Taiwan and its neighboring islands (Fig. 2). Besides providing improved detection, the digitally recorded data also made phase identification and picking more efficient. A dataset, consisting of seismograms recorded for three and a half years, can now be used for tomographically imaging the deep structure under the Taiwan area. We found the body-wave tomographic imaging method as formulated by Thurber [10,11] to be quite suitable for this work.

Insofar as Taiwan has been considered a typical example of arc–continent collision orogen [12], a thorough understanding of the physical environment in which the orogenic processes are taking place is obviously important. A tomographic study of the lithospheric structures under Taiwan will provide us not only important constraints on the modeling of the Taiwan orogeny in particular, but will also lead us to a general understanding of the plate interactions and mountain building.

2. Data and method

The seismograms used in this study are recorded by the combined Central Weather Bureau Seismic Network (CWBSN) and the Taiwan Telemetered Seismographic Network (TTSN); it has a total of 75 stations (see Fig. 2). Prior to 1994, the TTSN had one component (vertical) stations; they have since been merged into the CWBSN and now are all

equipped with three-component short-period sensors. Out of the total 24,312 events located by the combined network between March 1991 and July 1994, 1197 events were chosen for this study. The event selection criteria were: (1) the earthquakes having arrivals recorded at more than 8 stations; and (2) the largest azimuthal gap being less than 180° between stations, except for the deep events in the subduction zone immediately northeast of the island. The P and S arrival times for the events chosen were checked and reread, especially for events in the subduction zone under northern Taiwan.

In our inversion, the P-wave velocities at grid points in a three-dimensional space are sought. Because of the specific station and event locations given, a particular choice of 3-D grids will cause some space between grids to be illuminated and others untouched. In order to examine different tectonic features in more detail, three different grid configurations (Fig. 2) were set up for the velocity parameterization in the three-dimensional velocity inversion. They are: (a) a EW–NS oriented grid system for the northern third of Taiwan; (b) a grid system with the horizontal orthogonal directions parallel (N20°E–S20°W) and perpendicular (S70°E–N70°W) to the strike of the island in the northern two-thirds of Taiwan; and (c) a EW–NS grid system for the whole island. We modeled only P waves in the present study. The number of the earthquakes and P-wave arrivals used in this study for three different areas are shown in Table 1.

For each grid system, a one-dimensional velocity model is first obtained by a simultaneous inversion of both a layered velocity structure and the hypocentral locations [13], and it is used as the starting model for the tomographic inversion. In the simultaneous inversion [10,11,14], a damped, linear, least-squares inversion algorithm was used. Because the scale of computing involved is quite large, Pavlis and Booker's [15] method was used to decouple the hypocenter locations and the velocity structure determination in each step. Within each step we allow five iterations in the hypocenter location. The step is repeated until the result of the F-test shows that the change in variance is no longer significant; it usually takes six to seven steps. The velocity and its partial derivative at each discrete point in the 3-D model are calculated by linear interpolation from the surrounding eight grid points. The resulting velocity model is piecewise continuous and appropriate for modeling the complex tectonic environment in our study area. For the traveltime calculation, approximate ray-tracing algorithms were used to determine an initial minimum-time circular ray path connecting the source and receiver [10], and, through an iterative pseudo-bending approach [16], to adjust the ray path for a better approximation of the true path, which was in accord with the local velocity gradient.

To quantify the "goodness-of-fit" of the model parameters, the model standard error and spread function [17,18] are calculated. The model standard error is an estimate of how the data error is mapped

Table 1
Key parameters and results relevant to the 3-D inversions

Area	Number of Earthquakes	Number of P Arrivals	V_p Damping	Initial Weighted RMS residual (seconds)	Final Weighted RMS residual (seconds)
Northern Taiwan	510	8058	40	0.253	0.145
North-Central Taiwan	939	20,565	120	0.290	0.174
Whole Taiwan	1008	21,110	80	0.271	0.173

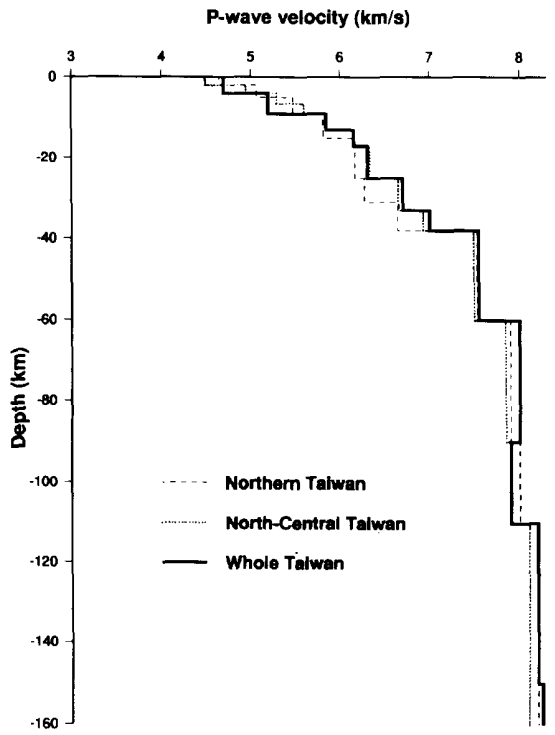

Fig. 3. One-dimensional P-wave velocity models for northern, north-central, and the whole of Taiwan obtained by simultaneous inversions for hypocenters and layer structures.

into the model error. A zero spread function implies a perfectly defined parameter, whereas large spread functions correspond to parameters having broad kernel shapes and small values of the resolving kernel.

To test the validity of our results, we ran inversions with a range of damping values. In the "spread-versus-the-standard-error" plot, the standard error initially decreases sharply when damping is increased, and then it decreases more slowly after the damping reaches a certain value. We define the optimum value for damping as a value in the vicinity of this transition. Thus, we seek compromise solutions that have a reasonable and standard error [17]. Solutions with damping values much lower than the adopted optimum value tend to be more oscillatory. For the inversions with the higher damping values, the velocity solution becomes highly smoothed.

3. Tomographic imaging results

The one-dimensional models obtained from 1-D inversions for the three selected grid configurations

Fig. 4. Tomographic profiles and their corresponding spread functions; the locations of the profiles are shown in Fig. 2a–c. The P-wave velocity distributions are shown on the left and the spread functions are shown on the right. The velocity contour interval is 0.5 km/s. ○ = relocated hypocenters including events within ±1 grid space of the profile; + = locations of the nodes. White areas mark unsampled regions. The topography corresponding to each profile is shown on top of the velocity section. *PS* = Philippine Sea; *ECER* = eastern Central Range; *IP* = Ilan Plain; *WCER* = western Central Range; *WF* = Western Foothills; *V* = Tatun volcano group; *CP* = Coastal Plain; *COR* = Coastal Range. Note that profiles are not plotted on the same scale; in particular, *B–B′* is plotted at about 50% of the other profiles-the hypocenters shown in *B–B′* appear to be smaller in comparison with those shown in other profiles.

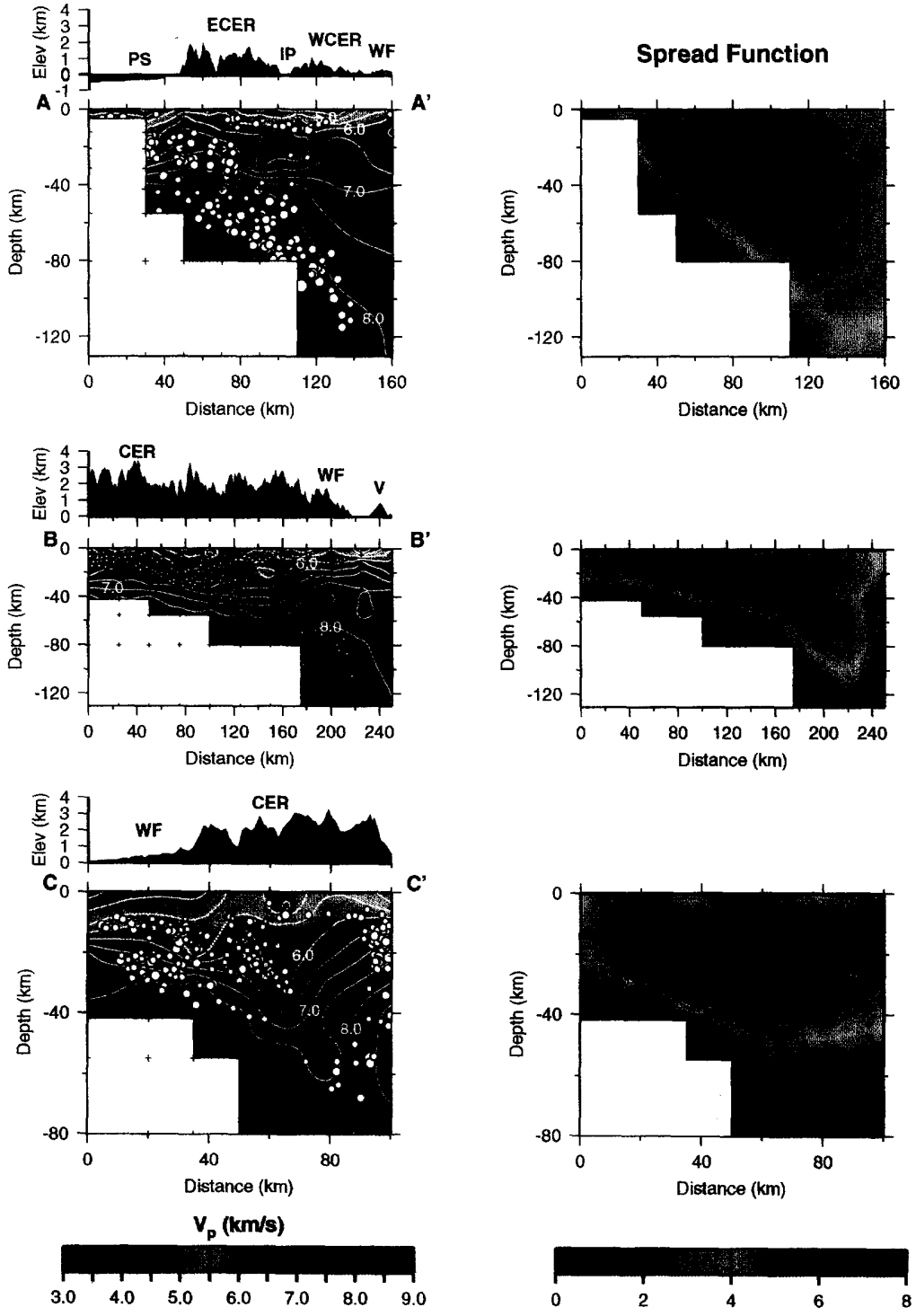
Spread Function
ECER
PS
IP
WCER
WF
A
A'
CER
WF
V
B
B'
CER
WF
C
C'
Elev (km)
Depth (km)
Distance (km)
6.0
7.0
8.0
V_p (km/s)
3.0 4.0 5.0 6.0 7.0 8.0 9.0
0 2 4 6 8

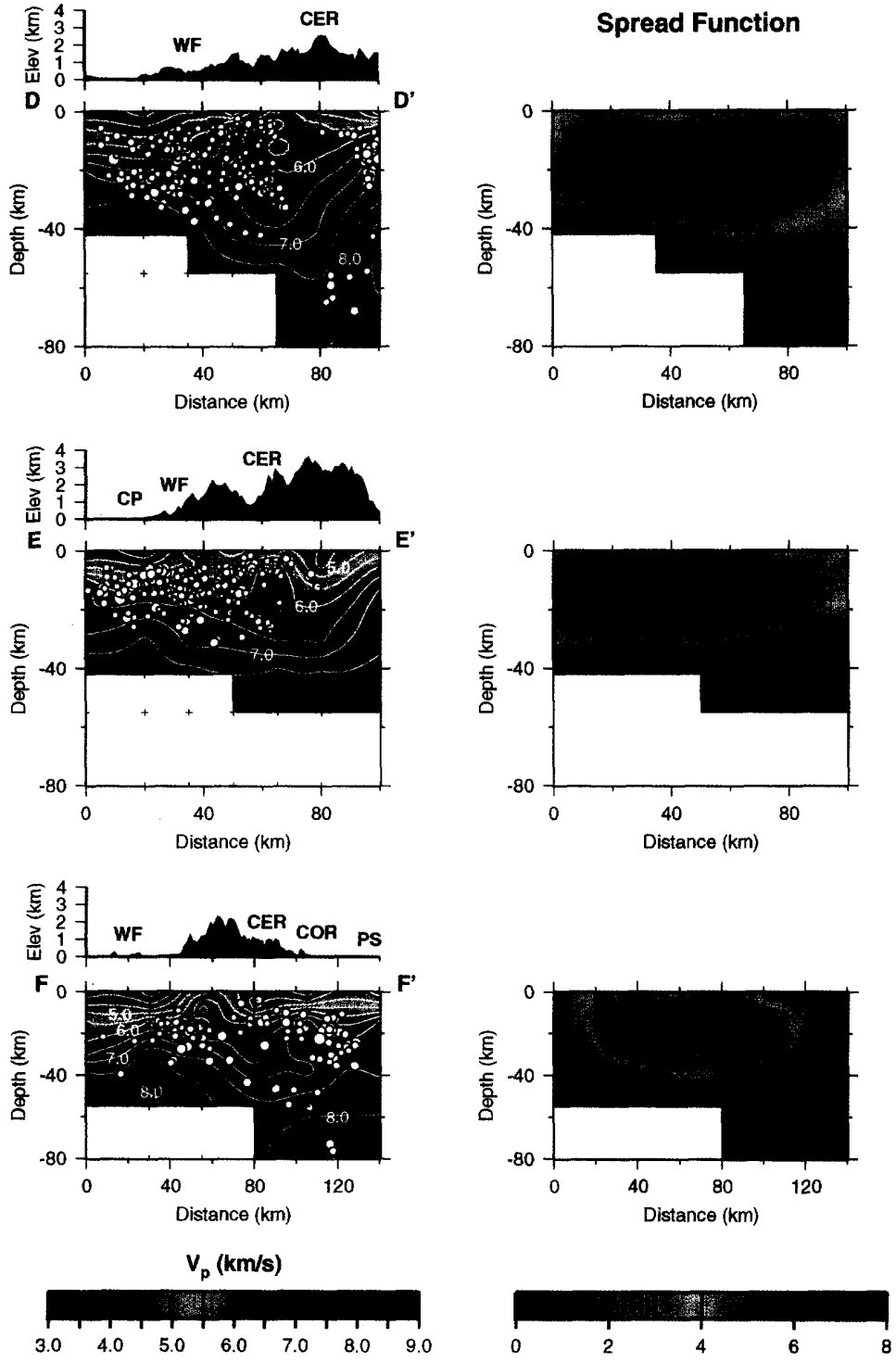

Fig. 4 (continued).

are shown in Fig. 3. The models for the northern two-thirds, and for the whole island are quite similar, as can be expected by the large overlap in their area coverage, although the events under the southern third of the island were not used in deriving the north-central Taiwan model. The northern Taiwan model is clearly different from the other two; 40 km can be taken as the Moho depth, where the P_n velocity is about 7.6 km/s. The weighted root mean square (RMS) arrival time residuals obtained using these 1-D models are 0.253, 0.290 and 0.271 s for northern Taiwan, north-central Taiwan and the whole island, respectively.

The 1-D models are used as initial models for our 3-D inversions. At the end of six to seven iterations, the RMS residuals decreased from the values listed above to 0.145, 0.174 and 0.173 s, respectively. These are slightly higher than the overall estimated reading error of 0.07 s. The optimal P-wave velocity damping values chosen are listed in Table 1 for the three different areas. For the final results, the calculated average model standard errors are 0.04, 0.02 and 0.02 km/s for the areas of northern Taiwan, north-central Taiwan and the whole Taiwan, respectively. These errors may underestimate the actual error by 100%, as shown by Thurber [19], using synthetic tests. Thus, the average errors in absolute velocity of the final models of the current study may range up to 0.04–0.08 km/s. For most of the earthquakes, the resulting hypocenters in our 3-D inversions deviate from their initial locations by less than 2 km horizontally and 5 km vertically. For earthquakes below 80 km, or just outside the seismic network, the deviation may be as much as 10 km horizontally and 15 km vertically. In terms of absolute locations, the average errors of earthquake location are 3 km horizontally and 5 km vertically. For some deeper earthquakes, and earthquakes occurring just outside the network, the location errors range up to 10 km horizontally and 15 km vertically.

Our 3-D results are displayed in a series of profiles; their positions are marked in Fig. 2a–c. The profiles (Fig. 4) are chosen to show the major variation in velocity structures under Taiwan. The hypocenters shown in Fig. 4 have been relocated. The spread function for each profile is also presented to provide a basis for judging the spatial resolution of the cross-section [18]. In this study, we consider the acceptable spread function to be 5.0. In each of the profiles and the spread function plot the white areas mark the unsampled regions.

3.1. Northern Taiwan profile (A–A′)

The most prominent feature in the subsurface P-wave image of northern Taiwan is the inclined high-velocity zone (*A–A′*, Fig. 4). In section *A–A′*, this zone is mapped at a depth range of 20–55 km, starting at about 45 km on the distance axis (corresponding to 24°N, 121.6°E), and continuing northward with a shallow dip ($< 20°$) for 40 km, before it dives more steeply northward with a dip of 40° from a depth range of 40–80 to 100–130 km. The velocities in the subduction zone are 8.0–8.4 km/s, or about 3–8% higher than the 1-D average starting model in the depth range of 40–130 km. Also clear in this profile is the low-velocity wedge above the high-velocity zone, ranging from 40 to 80 km in depth. The velocities within the wedge are about 6.9–7.5 km/s, or 4–8% lower than the 1-D model. Above the wedge is a crustal (< 30 km) low-velocity zone (5.7 km/s or -4% on the average), under the Ilan Plain of northern Taiwan. In the upper 10 km, high P-wave velocities (5.0–6.2 km/s or 4–12% higher than that of the 1-D model) are found under the eastern Central Range, where high-grade metamorphic rocks crop out, and low P-wave velocities (4.0–5.5 km/s, or 4–12% higher) are found under the western Central Range. Note that the Wadati-Benioff zone, as defined by seismicity, coincides with the inclined high-velocity zone under northern Taiwan; this correlation renders the straightforward interpretation of the high-velocity zone as the subduction zone.

3.2. S20°W–N20°E profile (B–B′) (along the ridge of the Central Range)

The northern end of this profile coincides with that of profile *A–A′*; it diverges by 20°, clockwise, from *A–A′*. The point at which this profile crosses the low-velocity wedge it is 15 km west of the corresponding point on profile *A–A′*. This profile clearly images the structures under the ridge of the Central Range. In the north (to the right of the 170–190 km mark in *B–B′*), the westward extension

of the N-dipping high-velocity zone and the low-velocity upper-mantle wedge observed in A–A' can be discerned. While the velocities in the high-velocity zone in the two profiles are about the same, the velocities in the low-velocity wedge in profile A–A' are noticeably lower than those in profile B–B' (-4 to -8% vs. 0 to -2%). The most striking features in B–B' are the thickening of the lower-velocity upper structures (above a depth of 40 to 55 km) under the higher elevations to the left of the 170 km mark along the distance axis and the gradual thinning of this structure further south (to the left in B–B', Fig. 4). The implication of this observation in terms of tectonics is quite interesting as will be discussed below. Earthquakes in this section occur diffusely in the upper 40 km and within the inclined high-velocity zone; the middle part of the Central Range and the low-velocity wedge, however, are nearly aseismic.

3.3. N70°W–S70°E profiles, C–C', D–D', E–E' and F–F' (perpendicular to the strike of the island)

The most prominent feature in these sections (profiles C–C' through F–F') is the thickening of the crust under the higher elevations of the Central Range, except in southern Taiwan (profile F–F'), where the deepest part is offset to the east. This thickening is much more pronounced in the north (C–C' and D–D') where low-velocity materials extend to a depth of about 75 km; this low-velocity feature was also observed to some extent by Roecker et al. [7], but due to the larger block size used in their work, the velocity contrasts are much attenuated. The high velocities below about 20 km in the eastern part of the C–C' and D–D' profiles are in sharp contrast to the low-velocity root in the west; the contact between them is quite steep. Toward the south, although the thickening is still substantial along profile E–E', it is noticeably less, and the lateral extent of the low-velocity crustal root is seen to have decreased in profile F–F', in comparison to the three profiles to the north. Also consistently seen in these profiles are the relatively high velocities in the top 15 km under the Central Range, relative to velocities under the Foothills and the Coastal Plain; the 5.5 km/s contours in all four profiles rise under some part of the Range, although not necessarily the highest part. The thickness of the low-velocity materials (< 5.0 km/s) under the Foothills and the Coastal Plain imaged in these sections remain nearly constant. The earthquakes shown in these sections occur mostly in the upper 40 km under the Western Foothills and in the top 40–70 km, being deeper toward the north, under the eastern Central Range. The middle part of the Central Range is nearly aseismic.

An additional feature in the eastern part of profile F–F' (Fig. 4) is the high-velocity zone, at a depth range of 15–50 km, under the Coastal Range and the Philippine Sea, between the 100 and 140 km marks on the distance axis. Note that the seismicity within this high-velocity zone is quite high. This profile is located just at the point where the subduction zone in southern Taiwan becomes visible based on seismicity. Thus, the high velocity observed at a depth range of 55–80 km in the eastern part of this profile may be related to this subduction zone; in fact, the seismicity shown in F–F' (Fig. 4) also suggests this relationship.

4. Discussions

The 3-D velocity structures under Taiwan obtained by tomographic inversion present details of the crust and upper mantle that are key to the understanding of Taiwan tectonics. Of the easily identified features, the inclined high-velocity zone under northern Taiwan (profiles A–A' and B–B', Fig. 4) evidently corresponds to the subduction zone mapped previously by seismicity alone. In these profiles, zones of high velocity and the seismicity superpose. The number of earthquakes in the western zone, however, is quite small, yet the increase in velocities in these two locations is roughly the same. In neither profile is the underside of the slabs well illuminated, because the first P arrivals travel through the high-velocity slab -this is a particular problem in using local earthquake data for tomography. In terms of studying the low-velocity wedge above the subduction zone, Taiwan provides an interesting locale. The back-arc basin is evidently alive, and probably very young, judging by the presence of $M > 6$ normal-faulting earthquakes in the southwestern terminus of the Okinawa Trough offshore of Ilan [1] and

the rapid subsidence of the Ilan Plain [20]. The area of low velocities in A–A' is more extensive and the values are lower than those in profile B–B', just 15 km to the west. Both profiles intersect areas with recent volcanism, but B–B' is placed to the west of the tip of the triangular-shaped Ilan Plain, not yet reached by the westward propagating Okinawa Trough. The juxtaposition of the low-velocity mantle wedge and the high-velocity slab is quite similar to those in the northwest Pacific [21], Alaska [22] and Japan [23]. Due to a lack of stations offshore of northern Taiwan, the northward extension of the mantle wedge cannot be mapped adequately along A–A', but in profile B–B' the velocity seems to increase near the northern end, signifying the termination of the low-velocity wedge.

One of the important questions in studying the Taiwan collision is the location of the trench near Taiwan. Since the compression is at its maximum where the two colliding plates are fully engaged, and it diminishes as the Philippine Sea Plate begins its northward subduction, this location determines where mountain building is taking place. Because of the disappearance of the bathymetric low associated with the Ryukyu Trench 100 km east of Taiwan, little evidence is available heretofore concerning the westward continuation of the Trench; it has been placed as far north as Suao [24], but, generally, it is believed to be near Hualien (e.g., [25]) (Fig. 1). Although seismicity defines the general plate configuration quite well, it is too diffuse for defining where the plate starts to bend. Also, between the end of the Ryukyu Trench and Taiwan there had not been any normal faulting earthquakes, which are associated with plate-bending near the trench [1]. By extrapolating the upper limit of the high-velocity zone to the south (A–A', Fig. 4), the intersection of the "trench" with the island is located by our tomographic results at approximately 23.8°N. The collision-induced orogeny should gradually diminish north of this point. It is gradual because the finite plate thickness ensures that the total disengagement of the subducting Philippine Sea plate from the Eurasian plate will take a finite distance to complete. With a plate thickness of 50 km and an average dip of 30°, say, it will take 100 km. The situation is schematically illustrated in Fig. 5, in which an idealized subduction zone is superposed on the velocity contours in profile B–B' (Fig. 4). The crosshatched area is the section in which the Eurasian and the Philippine Sea plates are fully engaged in collision, and to the north, where the subducting plate dives further into the upper mantle, no compression is exerted on the Eurasian plate.

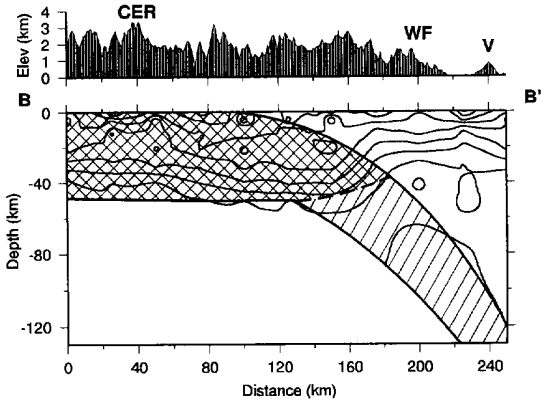

Fig. 5. Schematic diagram showing the position of the subducting Philippine Sea plate relative to the location of the mountains and its crustal root as indicated in profile $B-B'$ (Fig. 4). The subducting plate boundary is about 35 km east of the profile $B-B'$. The crosshatched area is the section in which the Eurasian and the Philippine Sea plates are fully engaged in collision. As the subducting plate dives further into the upper mantle, there is no longer any compression exerted on the Eurasian plate. Note that the average elevation on this profile remains nearly constant between 0 and 170 km on the distance axis. The elevation decreases gradually beyond 170 km.

Of great importance to the understanding of the Taiwan orogeny is the imaging of the relatively high-velocity region in the upper 10–15 km under the Central Range. In the "thin-skinned" modeling of Taiwan [6], the Central Range should be underlain by the deepest part of a tapered wedge consisting mainly of Tertiary sediments, and therefore should appear as a continuation of the upper-crustal low-velocity zone under the Western Foothills. In the images (Fig. 4) the upper-crustal high-velocity feature under the Central Range is seen to be continuous with the lower-crustal layer, which is generally thickened to form a "root" under the high elevations of the Central Range. Thus the formation of the

[1] Such an earthquake did take place on May 24, 1994, located at 24.04°N and 122.34°E (S. Sipkin, pers. commun., 1994).

Central Range appears to be resulting from up-arching of the pre-Tertiary basement and the lower-crustal materials, as well as the downwarping of the lower crust. In profile C–C', high-velocity materials are seen to extend to the surface on the eastern end of the profile, where pre-Tertiary high-grade metamorphic rocks crop out. The high-velocity zones under the eastern Central Range imaged in profiles C–C' and D–D' are somewhat intriguing. The velocities in these zones are similar to those in the high-velocity zone under the Western Foothills and the Central Range, but the fact that they start as shallow as 20 km and are next to the Philippine Sea plate makes us suspect they are part of the oceanic lithosphere. The seismicity in this zone is also notably higher than in its neighboring area to the west. In profiles C–C' and D–D' the low-velocity root is seen to be quite deep, with the 7.5 km/s contour at around 55–65 km. How these deep roots form is a question worth exploring. Was it formed simply by crustal thickening or did the thickening lead to the breaking of the upper mantle lid and thus allowing the intrusion of the asthenosphere? With available data we cannot answer these questions with any certainty, but with an accumulation of teleseismic P-wave data, recorded by the network since late 1994, it can be studied in the future.

The variation of the extent of the root can also be seen from profile B–B' (Fig. 4); using the 7.5 km/s contour as a marker, the root under the ridge of the Central Range is seen to decrease from a maximum of 55 km near the 160 km marker in B–B' to about 40 km near the southern end of the profile. It is commonly agreed that because of the obliqueness of the collision that created Taiwan, the orogeny started in the north and propagated southward [6,9]. Lee et al. [9] placed the initial contact near the northern end of the Coastal Range, starting at about 4 my BP, and the collision is now proceeding further south from the southern end of the Coastal Range. If so, we should expect the mountains in the north to be more mature, with perhaps more of an extensive root, than in the south (near Taitung, see Fig. 1). The slow decrease southward of the root is most probably an expression of this process.

To further understand the imaged lateral variations of seismic velocity in the upper mantle we need to evaluate the velocity changes due to changes in composition and melt content of the mantle material or from changes in ambient pressure and temperature. In terms of composition change, changes in V_p are related to the amount of basalt melt removal from the mantle. Studies [26,27] show that, with 10% basalt depletion, V_p increases by ~ 0.003 km/s for upper mantle rocks; this is negligibly small. However, a 3–6% melt by volume may lead to a 5–10% decrease in V_p [28], the aspect ratio of the cracks being the key factor determining the exact amount of variation. For the two ambient factors, temperature variations may cause a 0.04–0.06 km/s change in V_p per 100°C, based on $\partial V_p/\partial T = -3.93 \times 10^{-4}$ km/s/°C [29] and -6×10^{-4} km/s/°C [30]. At confining pressures from 6 kbar (~ 18 km) to 30 kbar (~ 90 km), variations in pressure may cause up to 0.015 km/s change in V_p per 1 kbar (~ 3 km) [30,31]. The preceding values are for mantle rocks.

For the subduction system in northern Taiwan (A–A', Fig. 4), the average absolute P-wave velocities are 8.2 km/s in the slab and 7.2 km/s in the mantle wedge (or +6% and −6% relative to the 1-D model) at depths of 50–100 km. The positive velocity anomaly can be explained readily by the subduction of cold lithosphere into the hot upper mantle. Given the Eurasian Plate–Philippine Sea Plate plate motion of 7.1 cm/yr in the direction of N50°W [3], the Philippine Sea Plate slab velocity is 3 cm/yr in the N20°E direction. Taking 40° as the dip and 60 km as the thickness of the slab, with values for other parameters and heat energy sources adapted from Creager and Jordan [32], the calculated average temperature contrast between the slab and the "normal" mantle is about 600°C at depths between 50 and 100 km, corresponding to a 0.24–0.36 km/s (3–5%) change in V_p. Intraplate deformation or escape of the Philippine Sea Plate [1] may speed up the subduction, but, even by increasing the slab velocity to 5–7 cm/yr, the temperature contrast will only increase by about 100°C, corresponding to a 0.04–0.06 km/s ($\sim 0.6\%$) change in V_p. Thus, with an initial V_p of 7.8–8.0 km/s at depths of 50–100 km, an increase of V_p to 8.3 km/s can easily be achieved.

In the thermal model described above, the calculated temperature of the mantle wedge has an average value of about 100°C less than the "normal mantle" at depths of 50 to 100 km, corresponding to

a 0.04–0.06 km/s change in V_p. This small amount of change in V_p cannot explain the observations (0.4–0.6 km/s changes in V_p) in the mantle wedge. In addition to the temperature contrast that lowers the V_p slightly, we must consider the effects of partial melting and water on V_p in the mantle wedge. For the effect of partial melt on V_p, 3–5% melt proportions are required for 0.4–0.6 km/s changes in V_p in the mantle wedge [28]; the exact amount is not resolvable because of the dependence of melt fraction on the morphology of the melts. For the effect of water on V_p, Ito [33] found that, at a pressure of 10 kbar and a temperature of 900°C, 5% drop of V_p can be explained by the presence of about 20 kg/m^3 water in the mantle rocks; the free water can be released by dehydration of the hydrous minerals derived from subducting slab [34]. Either one of these two factors provides a possible explanation to a lowered V_p in the mantle wedge.

5. Conclusion

Using seismic arrival time data accumulated in three and a half years, from the telemetered seismic network in Taiwan, clear images of velocity distributions in the crust and upper mantle under Taiwan have been obtained. The subduction zone under northern Taiwan was delineated and so was the low-velocity mantle wedge above it. Based on these results we are able to delineate the location of the "trench" for the subduction zone offshore of northern Taiwan and place a part of northern Taiwan above the low-velocity wedge. Also clearly shown in the images are the thickening of the crust under the Central Range and the presence of high-velocity materials at shallow depth under the Central Range. The extent of thickening decreases from Hualien southward as the mountain range becomes younger. If our interpretation is correct, it implies that the mountain building in Taiwan involves the participation of crust and upper mantle and it calls into question the appropriateness of the modeling of Taiwan orogeny in terms of thin-skinned tectonics.

Acknowledgements

We are grateful to Clifford H. Thurber, Donna Eberhart-Phillips, and Bill Ellsworth for providing their computer programs, to Ban-Yuan Kuo for discussions and assistance in computing temperature profiles, and to Wang-Ping Chen for many helpful comments on the manuscript. We also thank T.C. Shin and the staffs in the Central Weather Bureau Seismological Observation Center of Taiwan, ROC, for providing and discussing the earthquake data. Figures used in this study were generated from GMT-SYSTEM v. 2.1.4 [35]. Computations were done on the NSF/SUNY-funded SUN workstations. The text benefited from the constructive reviews of Chi-yuen Wang, Dapeng Zhao and Charles Langmuir. This research was supported by grant EAR-9206545 from the National Science Foundation. [*CL*]

References

[1] F.T. Wu, Recent tectonics of Taiwan, J. Phys. Earth 26(suppl.), S265–S299, 1978.
[2] R.J. Rau, Flexure modeling and Taiwan tectonics, Thesis, 131 pp, State Univ. New York, Binghamton, NY, 1992.
[3] T. Seno, S. Stein and A.E. Gripp, A model for the motion of the Philippine Sea plate consistent with NUVEL-1 and geological data, J. Geophys. Res. 98, 17,941–17,948, 1993.
[4] S. Tsao, T.C. Li, J.L. Tien, C.H. Chen, T.K. Liu and C.H. Chen, Illite crystallinity and fission-track ages along the east central cross-island highway of Taiwan, Acta Geol. Taiwan. 30, 45–64, 1992.
[5] S.B. Yu, D.D. Jackson, G.K. Yu and C.C. Liu, Dislocation model for crustal deformation in the Longitudinal Valley area, eastern Taiwan, Tectonophysics 183, 97–109, 1990.
[6] J. Suppe, Mechanics of mountain building in Taiwan, Mem. Geol. Soc. China 4, 67–89, 1981.
[7] S.W. Roecker, Y.H. Yeh and Y.B. Tsai, Three-dimensional P and S wave velocity structures beneath Taiwan: deep structure beneath an arc–continent collision, J. Geophys. Res. 92, 10,547–10,570, 1987.
[8] Y.H. Yeh, C.H. Lin and S.W. Roecker, A study of upper crustal structures beneath northeastern Taiwan: possible evidence for the western extension of Okinawa trough, Proc. Geol. Soc. China 32, 139–156, 1989.
[9] T.Q. Lee, C. Kissel, E. Barrier, C. Laj and W.R. Chi, Paleomagnetic evidence for a diachronic clockwise rotation of the Coastal Range, eastern Taiwan, Earth Planet. Sci. Lett. 104, 245–257, 1991.
[10] C.H. Thurber, Earthquake locations and three-dimension crustal structure in the Coyote Lake area, central California, J. Geophys. Res. 88, 8226–8236, 1983.
[11] C.H. Thurber, Local earthquake tomography: Velocities and V_p / V_s -Theory, in: Seismic Tomography: Theory and Practice, H.M. Iyer and K. Hirahara, eds., pp. 563–583, Chapman and Hall, London, 1993.

[12] J. Suppe, The active Taiwan mountain belt, in: The Anatomy of Mountain Ranges, J.P. Schaer and J. Rodgers, eds., pp. 277–293, Princeton Univ. Press, Princeton, NJ, 1987.
[13] W.L. Ellsworth, Three-dimensional structure of the crust and mantle beneath the island of Hawaii, Ph.D. thesis, 237 pp., Mass. Inst. Technol., Cambridge, MA, 1977.
[14] D. Eberhart-Phillips, Local earthquake tomography: earthquake source regions, in: Seismic Tomography: Theory and Practice, H.M. Iyer and K. Hirahara, eds., pp. 614–643, Chapman and Hall, London, 1993.
[15] G.L. Pavlis and J.R. Booker, The mixed discrete–continuous inversion problem: application to the simultaneous determination of earthquake hypocenters and velocity structure, J. Geophys. Res. 85, 4801–4810, 1980.
[16] J. Um and C.H. Thurber, A fast algorithm for two-point seismic ray tracing, Bull. Seismol. Soc. Am. 77, 972–986, 1987.
[17] W. Menke, Geophysical Data Analysis: Discrete Inverse Theory, 289 pp., Academic Press, New York, NY, 1989.
[18] D.R. Toomey and G.R. Foulger, Tomographic inversion of local earthquake data from the Hengill-Grensdalur central volcano complex, J. Geophys. Res. 94, 17,497–17,510, 1989.
[19] C.H. Thurber, Earth structure and earthquake locations in the Coyote Lake area, central California, Ph.D. thesis, 332 pp., Mass. Inst. Technol., Cambridge, MA, 1981.
[20] H. Chen, Crustal uplift and subsidence in Taiwan; an account based upon retriangulation results, Spec. Publ. Cent. Geol. Surv. 3, 127–140, 1984.
[21] R. van der Hilst, R. Engdahl, W. Spakman and G. Nolet, Tomographic imaging of subducted lithosphere below northwest Pacific island arcs, Nature 353, 37–43, 1991.
[22] E. Kissling and J.C. Lahr, Tomographic image of the Pacific slab under southern Alaska, Eclogae Geol. Helv. 84(2), 297–315, 1991.
[23] D. Zhao, A. Hasegawa and H. Kanamori, Deep structure of Japan subduction zone as derived from local, regional, and teleseismic events, J. Geophys. Res. 99, 22,313–22,329, 1994.
[24] J.F. Stephan, R. Blanchet, C. Rangin, B. Pelletier, J. Letouzey and C. Muller, Geodynamic evolution of the Taiwan–Luzon–Mindoro belt since the late Eocene, Mem. Geol. Soc. China 7, 69–90, 1986.
[25] J. Suppe, Kinematics of arc–continent collision, flipping of subduction, and back-arc spreading near Taiwan, Mem. Geol. Soc. China 6, 21–34, 1984.
[26] T.H. Jordan, Composition and development of the continental tectosphere, Nature 274, 544–548, 1978.
[27] T.H. Jordan, Mineralogies, densities and seismic velocities of garnet lherzolites and their geophysical implications, in: The Mantle Sample: Inclusions in Kimberlites and Other Volcanics, F.R. Boyd and H.O.A. Meyer, eds., pp. 1–14, Am. Geophys. Union, Washington, DC, 1979.
[28] G.R. Helffrich, S. Stein and B.J. Wood, Subduction zone thermal structure and mineralogy and their relationship to seismic wave reflections and conversions at the slab/mantle interface, J. Geophys. Res. 94, 753–763, 1989.
[29] H. Kern, P-and S-wave velocities in crustal and mantle rocks under the simultaneous action of high confining pressure and high temperature and the effect of the rock microstructure, in: High-Pressure Researches in Geoscience, W. Schreyer, ed., pp. 15–45, Schweizerbart, Stuttgart, 1982.
[30] D.M. Fountain and N.I. Christensen, Composition of the continental crust and upper mantle; a review, Geol. Soc. Am. Mem. 172, 711–742, 1989.
[31] N.I. Christensen, Compressional wave velocities in possible mantle rocks to pressures of 30 kilobars, J. Geophys. Res. 79, 407–412, 1974.
[32] K.C. Creager and T.H. Jordan, Slab penetration into the lower mantle beneath the Mariana and other island arcs of the northwest Pacific, J. Geophys. Res. 91, 3573–3589, 1986.
[33] K. Ito, Effects of H_2O on elastic wave velocities in ultrabasic rocks at 900°C under 1 Gpa, Phys. Earth Planet. Inter. 61, 260–268, 1990.
[34] Y. Tatsumi, Migration of fluid phases and genesis of basalt magmas in subduction zones, J. Geophys. Res. 94, 4697–4707, 1989.
[35] P. Wessel and W.H.F. Smith, Free software helps map and display data, EOS Trans. Am. Geophys. Union 72, 441, 1991.